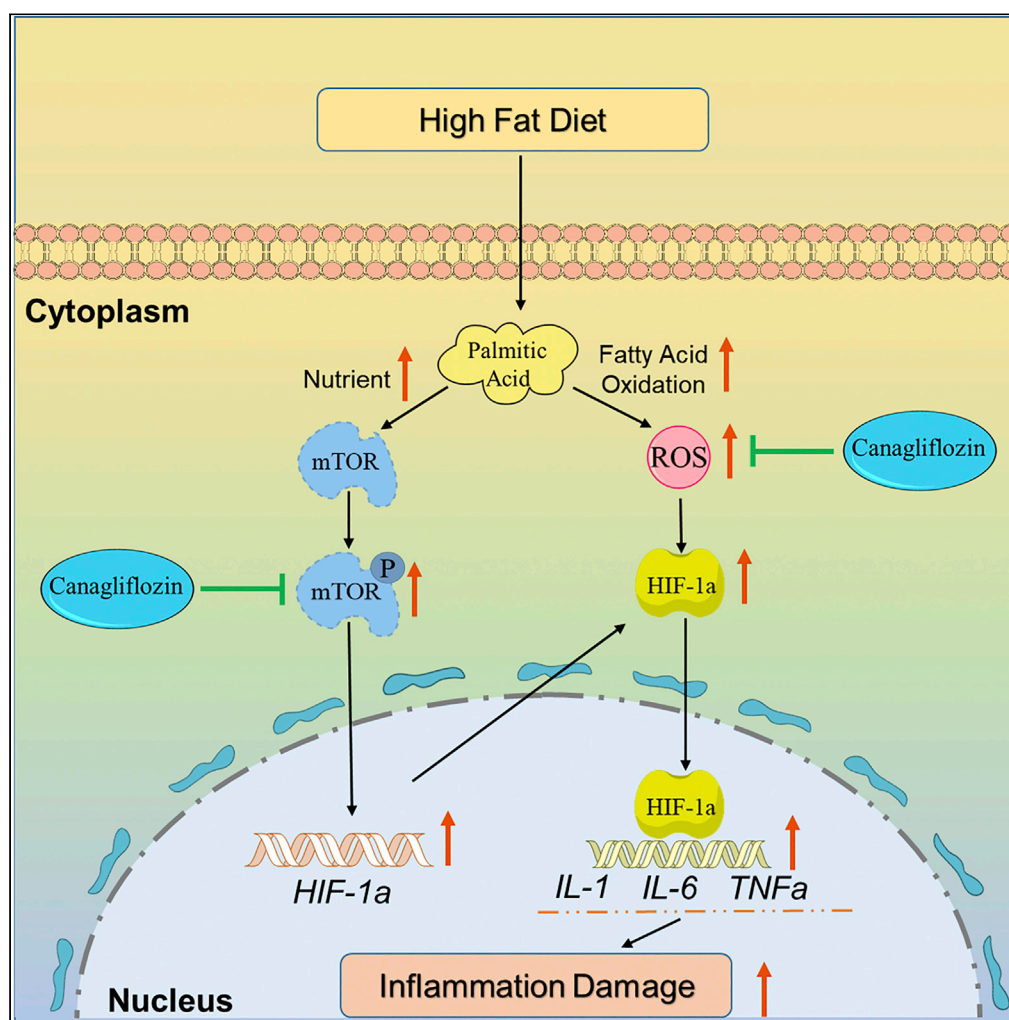## Article

Canagliflozin attenuates lipotoxicity in cardiomyocytes and protects diabetic mouse hearts by inhibiting the mTOR/HIF-1α pathway

Pengbo Sun, Yangyang Wang, Yipei Ding, ..., Naihan Xu, Yaou Zhang, Weidong Xie

xiewd@sz.tsinghua.edu.cn

Highlights

Canagliflozin ameliorated heart dysfunctions in HFD/STZ-induced diabetic mice

Canagliflozin inhibited lipotoxicity in palmitic acid-induced HL-1 cardiomyocytes

mTOR-HIF-1α pathway mediated lipotoxicity in cardiomyocytes

Canagliflozin bound to mTOR and inhibited mTOR-HIF-1α pathway

iScience

Article

Canagliflozin attenuates lipotoxicity in cardiomyocytes and protects diabetic mouse hearts by inhibiting the mTOR/HIF-1α pathway

Pengbo Sun,[1,2,3,4] Yangyang Wang,[1,2,3,4] Yipei Ding,[2,3] Jingyi Luo,[2,3] Jin Zhong,[1,2,3] Naihan Xu,[1,2,3] Yaou Zhang,[1,2,3] and Weidong Xie[1,2,3,5,*]

SUMMARY

Lipotoxicity plays an important role in the development of diabetic heart failure (HF). Canagliflozin (CAN), a marketed sodium-glucose co-transporter 2 inhibitor, has significantly beneficial effects on HF. In this study, we evaluated the protective effects and mechanism of CAN in the hearts of C57BL/6J mice induced by high-fat diet/streptozotocin (HFD/STZ) for 12 weeks *in vivo* and in HL-1 cells (a type of mouse cardiomyocyte line) induced by palmitic acid (PA) *in vitro*. The results showed that CAN significantly ameliorated heart functions and inflammatory responses in the hearts of the HFD/STZ-induced diabetic mice. CAN significantly attenuated the inflammatory injury induced by PA in the HL-1 cells. Furthermore, CAN seemed to bind to the mammalian target of rapamycin (mTOR) and then inhibit mTOR phosphorylation and hypoxia-inducible factor-1α (HIF-1α) expression. These results indicated that CAN might attenuate lipotoxicity in cardiomyocytes by inhibiting the mTOR/HIF-1α pathway and then show protective effects on diabetic hearts.

INTRODUCTION

Diabetes is a chronic metabolic disorder, characterized by hyperglycemia and complications caused by insulin deficiency and/or resistance. Cardiovascular complications are a major cause of mortality and morbidity in diabetic patients. Diabetic patients have an increased risk of cardiovascular mortality by 86%, and increased incidence rate of hospitalization for congestive heart failure (HF) by 185% compared with these factors in non-diabetic patients (Heintjes et al., 2019). In the absence of overt myocardial ischemia and hypertension, diabetes independently causes changes in the myocardial structure and function, which is known as diabetic cardiomyopathy (Bugger and Abel, 2014). Diabetic cardiomyopathy is one of the important causes for the development of HF. However, the potential pathological mechanisms of diabetic cardiomyopathy remain unclear.

A healthy heart requires a large amount of ATP to maintain normal function, and approximately 70% ATP is produced by fatty acid oxidation (FAO) (Lopaschuk et al., 1994). However, in diabetic hearts, mitochondrial dysfunction leads to fatty acid metabolic disorder, and increased lipid accumulation and oxidation, which lead to increased oxidative stress, inflammation, and lipotoxicity (Fillmore et al., 2014). Previous research also showed that increased myocardial triglyceride content in diabetic patients was associated with impaired left ventricular diastolic function (Rijzewijk et al., 2008).

Inhibiting lipotoxicity in the hearts of diabetic patients is a potential strategy for the treatment of diabetic cardiomyopathy and subsequent HF. However, currently there is not a suitable drug to attenuate lipotoxicity in the hearts of diabetic patients. Canagliflozin (CAN) is a sodium-glucose co-transporter 2 (SGLT2) inhibitor and is an antidiabetic drug. Clinical research has found that it has extra beneficial effects by decreasing hospitalization and mortality rates of HF in patients with type 2 diabetes mellitus (Rådholm et al., 2018). Furthermore, some studies have indicated that CAN may exert its cardioprotective effect independent of its hypoglycemic activity (Lim et al., 2019). CAN also improved lipid metabolism and attenuated the development of non-alcoholic fatty liver disease (Inoue et al., 2019). However, whether CAN regulated lipid metabolism and attenuated lipotoxicity in the hearts of diabetic patients remains unclear.

[1]Open FIESTA Center, Shenzhen International Graduate School, Tsinghua University, Shenzhen 518055, China

[2]State Key Laboratory of Chemical Oncogenomic, Shenzhen International Graduate School, Tsinghua University, Shenzhen 518055, China

[3]Key Lab in Health Science and Technology, Institute of Biopharmaceutical and Health Engineering, Shenzhen International Graduate School, Tsinghua University, Shenzhen 518055, China

[4]These authors contributed equally

[5]Lead contact

*Correspondence: xiewd@sz.tsinghua.edu.cn

https://doi.org/10.1016/j.isci.2021.102521

Mammalian target of rapamycin (mTOR) and hypoxia-inducible factor-1α (HIF-1α) are important factors mediating the pathological progression of HF in patients with diabetes (Kumar et al., 2018; Sanches-Silva et al., 2020). mTOR, as an energy metabolism factor, was also found to regulate HIF-1α expression (Land and Tee, 2007). However, no suitable drugs have been found to target the mTOR-HIF-1α pathway or to treat diabetic cardiomyopathy or HF. In this study, we aimed to evaluate the protective effects of CAN in a high-fat diet/streptozotocin (HFD/STZ)-induced diabetic HF mouse model and in palmitic acid (PA)-induced HL-1 cell lipotoxicity and investigate whether CAN targeted the mTOR-HIF-1α pathway to exert a cardioprotective effect.

RESULTS

The beneficial effects of CAN on body/adipose weight, blood lipid/glucose level, and heart lipid/glucose accumulation in HFD/STZ-induced diabetic mice

An unhealthy lifestyle has caused a significant increase in the morbidity and mortality rates in patients with diabetic complications, and the excessive intake of saturated fatty acids is one of the strongest risk factors in diabetic cardiovascular disease. Multiple mechanisms have been associated with the development of diabetic cardiovascular complications, such as oxidative stress, inflammation, and cell apoptosis (Liu et al., 2014). In this study, we first used HFD/STZ to induce a type 2 diabetic HF model in the C57BL/6J mice, and these were treated with CAN (25 mg/kg/day) for 12 weeks. During the experiment, the body weight of the HFD/STZ diabetic group was significantly increased at 1, 2, 5, 8, 9, and 11 weeks compared with that in the normal control group (Figure 1A). However, CAN significantly inhibited this increase at 3–12 weeks compared with that in the HFD/STZ diabetic control group. We also monitored the diet and water intake of the different groups (Figures 1B and 1C). There was a slight increase in the diet and water intake in the CAN-treated HFD/STZ diabetic group compared with that in the HFD/STZ diabetic control group. However, the HFD/STZ diabetic group showed a significant increase in the abdominal adipose tissue index (abdominal adipose tissue weight/body weight) compared with that in the normal control group, and this increase was significantly inhibited by CAN (Figure 1D). Therefore the body and adipose tissue weights reduced by CAN were not associated with the inhibition of dietary energy intake.

Subsequently, we evaluated the effects of CAN on glucose and lipid levels in the blood serum of the HFD/STZ diabetic HF model. The concentrations of triglycerides, cholesterol, and glucose in the serum showed a significant increase in the HFD/STZ diabetic group compared with that in the normal control group. However, CAN significantly attenuated this increase in the HFD/STZ-induced diabetic group (Figures 1E–1G). In addition, we evaluated the effects of CAN on glucose and lipid levels in the heart tissue. The increased concentrations of triglycerides, cholesterol, and glycogen in the heart tissues of the HFD/STZ diabetic group were also significantly inhibited by CAN (Figures 1H–1J). However, these beneficial effects of CAN on glucose and lipid metabolism in the serum and heart tissue were not associated with the regulation of dietary intake.

The protective effect of CAN on HF and metabolic inflammation induced by HFD/STZ *in vivo*

The progression of HF is accompanied by cardiomyocyte remodeling and fibrosis. Left ventricular hypertrophy and blunt heart apical are two notable morphological features (O'Grady et al., 2019). The heart morphological features in the HFD/STZ group were changed: left ventricular hypertrophy developed, the ventricular wall thickened, and the heart apical became blunt compared with that in the normal group; however, the heart shape was improved in the CAN group compared with that in the HFD/STZ control group after 12 weeks of treatment (Figures 2A and 2D–2F). We calculated the diameter of the cell in heart tissues by wheat germ agglutinin (WGA) staining; the HFD/STZ group had a hypertrophic cardiomyocyte compared with the normal control group (Figure 2B), whereas CAN significantly reduced the size of cardiomyocyte. This finding indicated that CAN inhibited myocardial hypertrophy *in vivo*. We also observed fibrosis in the cardiomyocytes in the different groups using Masson staining. Compared with that in the normal control group, the cardiomyocytes in the HFD/STZ group were arranged in a disorderly manner and were accompanied with notable fibrosis; however, these pathological changes were also reversed after CAN treatment (Figure 2C). In addition, we evaluated the heart ejection fraction in different groups, the HFD/STZ group had notable decrease of heart ejection fraction compared with the normal control group, but CAN treatment ameliorated this function (Figure 2G).

The serum B-type natriuretic peptide (BNP), creatine kinase (CK), and lactate dehydrogenase (LDH) levels are three key blood biochemical indexes used in the clinical diagnosis of HF that indicate abnormal left
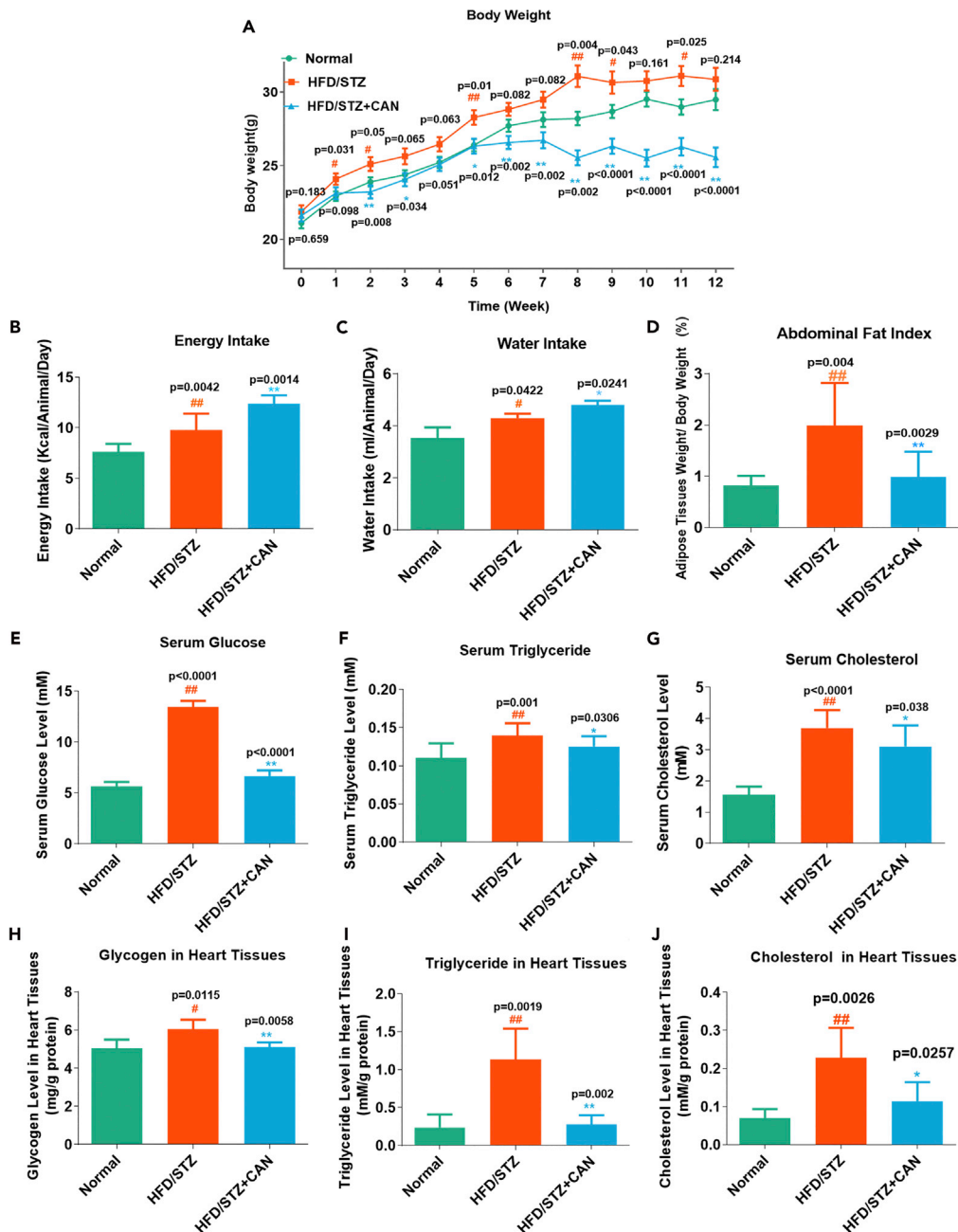
Figure 1. CAN reduced the body and adipose tissue weights, blood lipid/glucose levels, and heart lipid/glucose accumulation, which was not mediated by inhibiting the dietary intake in the HFD/STZ-induced C57BL/6 mice

(A–J) (A) Body weight, (B) energy intake (n = 8), (C) water intake (n = 3), and (D) adipose tissue weight index (n = 10), and (E) serum glucose (n = 10), (F) serum triglyceride (n = 10), (G) serum cholesterol (n = 10), (H) glycogen (n = 5), (I) triglyceride (n = 5), and (J) cholesterol levels in the heart tissues (n = 5) from the HFD/STZ-induced diabetic mice. Data are presented as the mean ± SD (n = 10). [#]$p < 0.05$ and [##]$p < 0.01$ versus normal; *$p < 0.05$ and **$p < 0.01$ versus HFD/STZ. Normal, normal control group; HFD, high-fat diet; STZ, streptozotocin; CAN, canagliflozin; HFD/STZ, HFD/STZ-induced diabetic control group; HFD/STZ + CAN, canagliflozin-treated HFD/STZ-induced diabetic group.

ventricular volume and myocardial injury (Nalban et al., 2020). We analyzed the heart morphological features using pathological staining and also detected the blood biochemical indexes (i.e., BNP, CK, and LDH) to confirm the effects of CAN against HF observed during clinical diagnosis. The serum BNP level was moderately increased in the HFD/STZ control group compared with the normal control group;
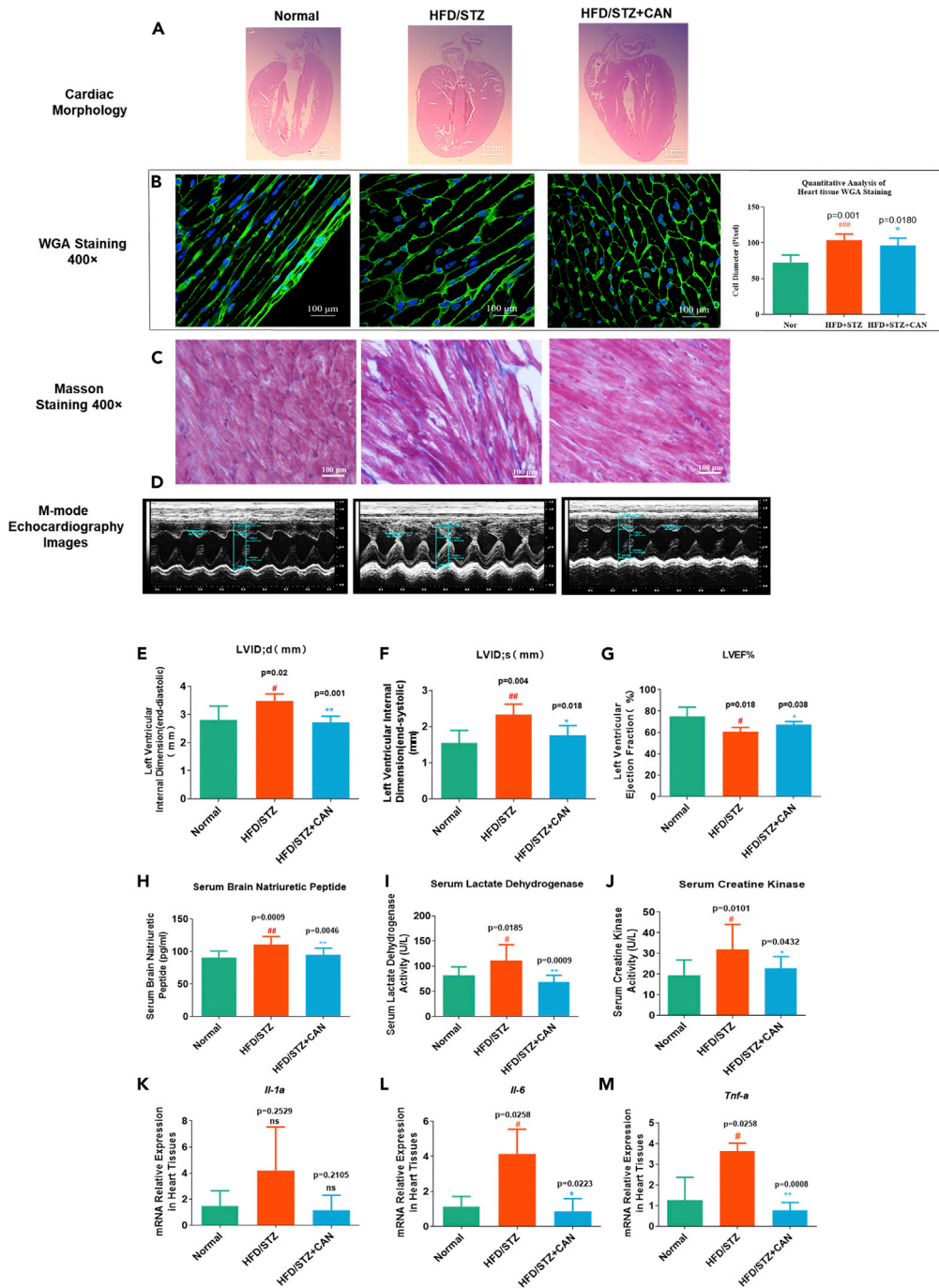
Figure 2. Protective effects of CAN in the hearts of HFD/STZ-induced diabetic mice

(A) Morphology of the hearts from the HFD/STZ-induced diabetic mice was measured using pathological slices.

(B and C) (B) WGA and (C) Masson staining using pathological slices in the hearts of the HFD/STZ-induced diabetic mice.

(D–F) (D) Representative M-mode echocardiographic images; (E) left ventricular internal diastolic diameter (LVIDd), (F) left ventricular internal systolic diameter (LVIDs), and (G) ejection fraction detected by echocardiography (n = 4–5).

(H–M) (H) BNP, (I) CK, and (J) LDH levels in the serum detected by biochemical kits (n = 10). mRNA expression levels of the inflammatory factors, (K) $Il-1\alpha$, (L) $Il-6$, and (M) $Tnf-\alpha$ in the hearts of the HFD/STZ-induced diabetic mice were determined using reverse transcription-quantitative PCR (n = 3). Data are presented as the mean $\pm$ SD. [#]p < 0.05 and [##]p < 0.01 versus

Figure 2. *Continued*

normal; *p < 0.05 and **p < 0.01 versus HFD/STZ. H&E, hematoxylin and eosin; BNP, B-type natriuretic peptide; CK, creatine kinase; LDH, lactate dehydrogenase; HFD, high-fat diet; STZ, streptozotocin; CAN, canagliflozin; normal, normal control group. HFD/STZ, HFD/STZ-induced diabetic control group; HFD/STZ + CAN, canagliflozin-treated HFD/STZ-induced diabetic group.

however, this increase was attenuated by CAN (Figure 2H). The serum CK and LDH levels in the HFD/STZ group were moderately increased compared with those in the normal control group. However, CAN significantly attenuated the increased CK and LDH levels in the HFD/STZ diabetic control group after 12 weeks of treatment (Figures 2I and 2J).

Inflammation plays an important role in diabetic HF development (Rana et al., 2007; Aimo et al., 2020). The increased tumor necrosis factor (TNF)-α, interleukin (IL)-1, and IL-6 levels are an important pathological characteristic in patients with HF (Zhang et al., 2017; Jones and Patel, 2018). We extracted the total mRNA from the cardiac tissues and detected the mRNA expression levels of the inflammatory cytokines, *Il-1α*, *Il-6*, and *Tnf-α* (Table 1) in the HFD/STZ-induced diabetic mice (Figure 2K–2M). The results showed that inflammatory mRNA *Il-6* and *Tnf-α* in the heart tissue of the HFD/STZ diabetic group were increased by 2- to 3-fold (Figures 2L and 2M) compared with that in the normal control group. However, this increase was significantly decreased after CAN treatment.

The protective effect of CAN on PA-induced HL-1 cell oxidative stress, inflammation, and apoptosis *in vitro*

PA is a saturated fatty acid that could induce cardiomyocyte inflammation, oxidative stress, and apoptosis *in vitro* (Mangali et al., 2019). To investigate cardiomyocyte oxidative stress, inflammation, and lipotoxicity *in vivo*, induced by HFD, we used the PA-treated myocardial cell line HL-1 and evaluated the protective effects of CAN on PA-induced cell hypertrophy, cell viability, oxidative stress, and inflammatory damage. PA significantly increased cell hypertrophy induced by PA *in vitro*, and CAN significantly inhibited cell hypertrophy through WGA analysis (Figure 3C). Reactive oxygen species (ROS) was used to evaluate oxidative stress and also apoptosis. PA significantly promoted the production of ROS in the HL-1 cells; however, CAN significantly attenuated the generation of ROS (Figure 3B). Methylthiazolyldiphenyl-tetrazolium bromide (MTT) assays indicated that cell viability was significantly lower in cells treated with PA compared with the normal control group, but that CAN significantly attenuated this effect (Figure 3D). LDH accumulation is an important pathological characteristic in cardiomyocyte damage. Therefore, we detected LDH activity from the HL-1 cell medium in the different experimental groups. The results showed that the LDH activity in the PA-treated cells was higher compared with that in the normal control group, but CAN significantly decreased LDH accumulation in PA-treated cells (Figure 3E). Furthermore, flow cytometry analysis showed that CAN could inhibit necrosis and apoptosis induced by PA (Figures 3I and 3J). These results indicated that PA lowered cell viability caused by lipotoxicity, but that CAN exerted protective effects. Following this we treated the HL-1 cells with CAN for 24 h and then detected the mRNA expression levels of inflammatory cytokines. RT-qPCR assays found that PA significantly induced the mRNA expression levels of *Il-1α*, *Il-6*, and *Tnf-α* compared with that in the normal control groups; however, this increase was significantly inhibited by CAN, in a dose-dependent manner (Figures 3F–3H). These results were consistent with the results *in vivo*. Notably, we found that CAN could inhibit HL-1 cell viability, oxidative stress, and inflammatory damage; however, CAN could not significantly reduce lipid accumulation in the HL-1 cells induced by PA (Figure 3A). These results indicated that CAN directly inhibited cardiomyocyte cell lipotoxicity *in vitro* and *in vivo*; however, this was not completely dependent on the regulation of lipid metabolism.

CAN exerted protective effects likely through HIF-1 signaling pathway

CAN is a selective SGLT2 inhibitor, and we proved its significant protective effects on lipotoxicity in cardiocytes induced by HFD and a fatty acid *in vivo* and *in vitro*, respectively, in this research. These results might explain the beneficial effects of CAN in patients with diabetic HF in clinical research. However, the potential molecular mechanisms remained unclear. SwissTargetPred5iction is a web server to predict the drug target for small molecules; it was used in this study, and the results revealed 102 possible targets of CAN (Data S1). Next, we analyzed the 102 possible targets using ClueGo, and the top 20 enriched signaling pathways are shown in Figure 4A. There were 13,747 diabetes-related genes and 12,522 HF-related genes identified using GeneCards, and the enriched pathways of top 200 genes were subsequently analyzed using ClueGo (Data S1). The top 20 diabetes and HF-related pathways are shown in Figures 4B and 4C, respectively.
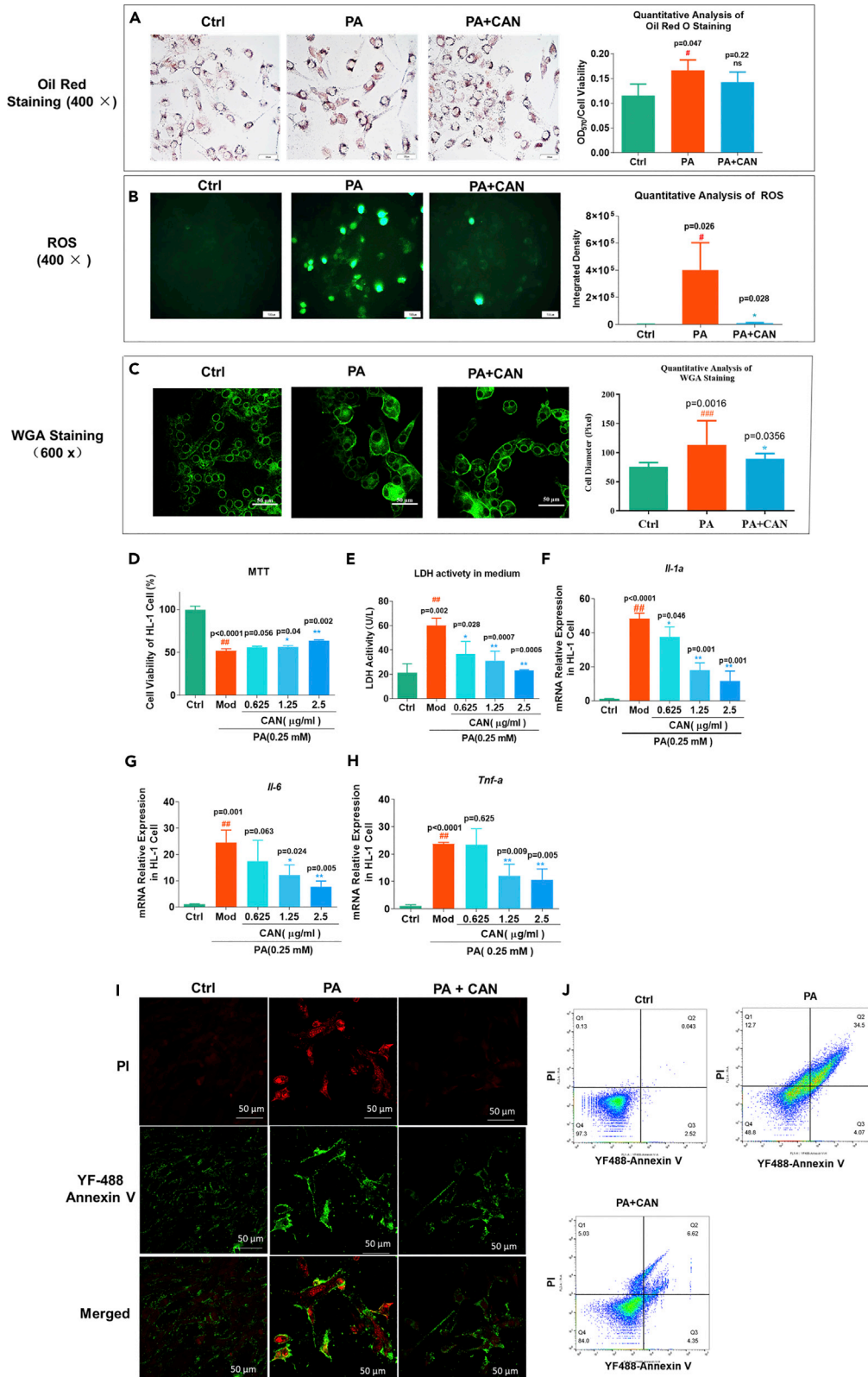
Figure 3. The protective effects of CAN on PA-induced HL-1 cell

(A) Oil red O staining results of the HL-1 cell line and quantitative analysis. Magnification, ×400.

(B) ROS was detected using the fluorescent probe, 2′,7′-dichlorofluorescein diacetate and quantitative analysis. Magnification, ×400.

(C) WGA staining results of the HL-1 cells after different treatments.

(D) Cell viability in the HL-1 cells was detected using MTT assay.

(E–H) (E) LDH activity in the HL-1 cell culture medium. mRNA expression levels of the inflammatory factors, (F) $Il\text{-}1\alpha$, (G) $Il\text{-}6$, and (H) $Tnf\text{-}\alpha$ in the HL-1 cells determined using reverse transcriptase-quantitative PCR.

(I) Immunofluorescence staining with YF488-Annexin V and PI in the HL-1 cells, using a confocal microscope (magnification, ×600). Red fluorescence indicates PI, green fluorescence indicates YF488-annexin V, and the merged figure indicates the merged signal of PI and YF488-annexin V.

(J) Flow cytometry assay in the HL-1 cells. Data are presented as mean $\pm$ SD (n = 3). $^{\#}p < 0.05$ and $^{\#\#}p < 0.01$ versus ctrl; $^{*}p < 0.05$ and $^{**}p < 0.01$ versus PA. Ctrl, untreated normal control; Mod/PA, PA-treated (0.25 mM) control group; 0.625, HL-1 cells were treated with PA (0.25 mM) and CAN (0.625 µg/mL); 1.25, HL-1 cells were treated with PA (0.25 mM) and CAN (1.25 µg/mL); 2.5, HL-1 cells were treated with PA (0.25 mM) and CAN (2.5 µg/mL); PA + CAN, HL-1 cells treated with PA (0.25 mM) and CAN (2.5 µg/mL); ROS, reactive oxygen species; LDH, lactate dehydrogenase; PA, palmitic acid; CAN, canagliflozin.

The common or overlapping pathways identified in Figures 4A–4C were analyzed using the Venn Graph Application in Origin Pro 2018c (Figure 4D, see also Data S1). We found that the HIF-1 signaling pathway was a common signaling pathway and might be the potential target pathway of CAN in clinical diabetic HF treatment (Figure 4D).

CAN inhibited mTOR phosphorylation in the HIF-1 signaling pathway *in vivo* and *in vitro*

Based on the aforementioned bioinformatics analysis, we selected the HIF-1 signaling pathway for the preliminary investigation. HIF-1α is a key target and plays an important role in oxidative stress, inflammation, and cardiovascular disease (Abe et al., 2017). We first detected the HIF-1α mRNA and protein expression levels *in vivo* and *in vitro* to verify the prediction. The results showed that higher levels of HIF-1α protein and mRNA expression were observed in the hearts of the HFD/STZ-induced diabetic mice compared with that in the normal control group, but CAN could inhibit this effect *in vivo* (Figures 5A, 5C, and 5D, see also Data S2). PA increased HIF-1α mRNA and protein expression level compared with that in the blank control group; however, CAN significantly reduced the HIF-1α mRNA and protein expression levels, in a dose-dependent manner, compared with that in the PA-treated group (Figures 5B, 5F, and 5G, see also Data S2) *in vitro*. As the HIF-1a mRNA expression level was changed significantly, CAN might inhibit HIF-1a expression by affecting an upstream target of HIF-1a in the HIF-1 signaling pathway. mTOR is an important mediator in cell metabolism, autophagy, and inflammation. mTOR phosphorylation and activation was found to regulate HIF-1α transcription in the HIF-1 signaling pathway (Land and Tee, 2007). Therefore, we next detected mTOR and p-mTOR (Ser 2448) protein expression levels in the HL-1 cell line and in the heart tissue from the HFD/STZ-induced diabetic mouse model. The *in vivo* results proved our hypothesis that CAN could inhibit the increase in mTOR phosphorylation in the HFD/STZ-induced mouse hearts (Figures 5A and 5E, see also Data S2) and in PA-treated HL-1 cell (Figures 5B and 5H, see also Data S2). We further confirmed that CAN inhibited mTOR phosphorylation using the immunofluorescence assay; CAN inhibited mTOR phosphorylation and further inhibited HIF-1α protein expression level in PA-treated HL-1 cell (Figure 5I). We have proved that CAN could inhibit HIF-1α expression level by inhibiting mTOR phosphorylation. However, whether mTOR was the potential target of CAN in the HIF-1 signaling pathway requires further investigation.

CAN might inhibit mTOR phosphorylation by binding to mTOR directly in the HIF-1 signaling pathway

Next, we investigated the potential interaction between CAN and mTOR using affinity chromatography and molecular docking. RAPA is an mTOR inhibitor and inhibits mTOR phosphorylation by binding to the FKBP-RAPA-binding (FRB) domain within mTOR (Marz et al., 2013). We compared the affinity and binding site of CAN and RAPA to the FRB domain of mTOR using SwissDock. The results showed that CAN and RAPA could bind to the same region of the mTOR FRB domain (Figures 6A–6E, see also Data S1), a hydrophobic pocket, which is composed of GLN49, TRP9, ILE7, and Arg4 amino acids, with similar predicted affinity (Gibbs free energy) (Figure 6F, see also Data S1). Subsequently, we verified the interaction between CAN and mTOR using affinity chromatography and western blot analysis. The results showed that CAN and mTOR might have a physical interaction with each other (Figures 6A and 6B, see also Data S2). These results
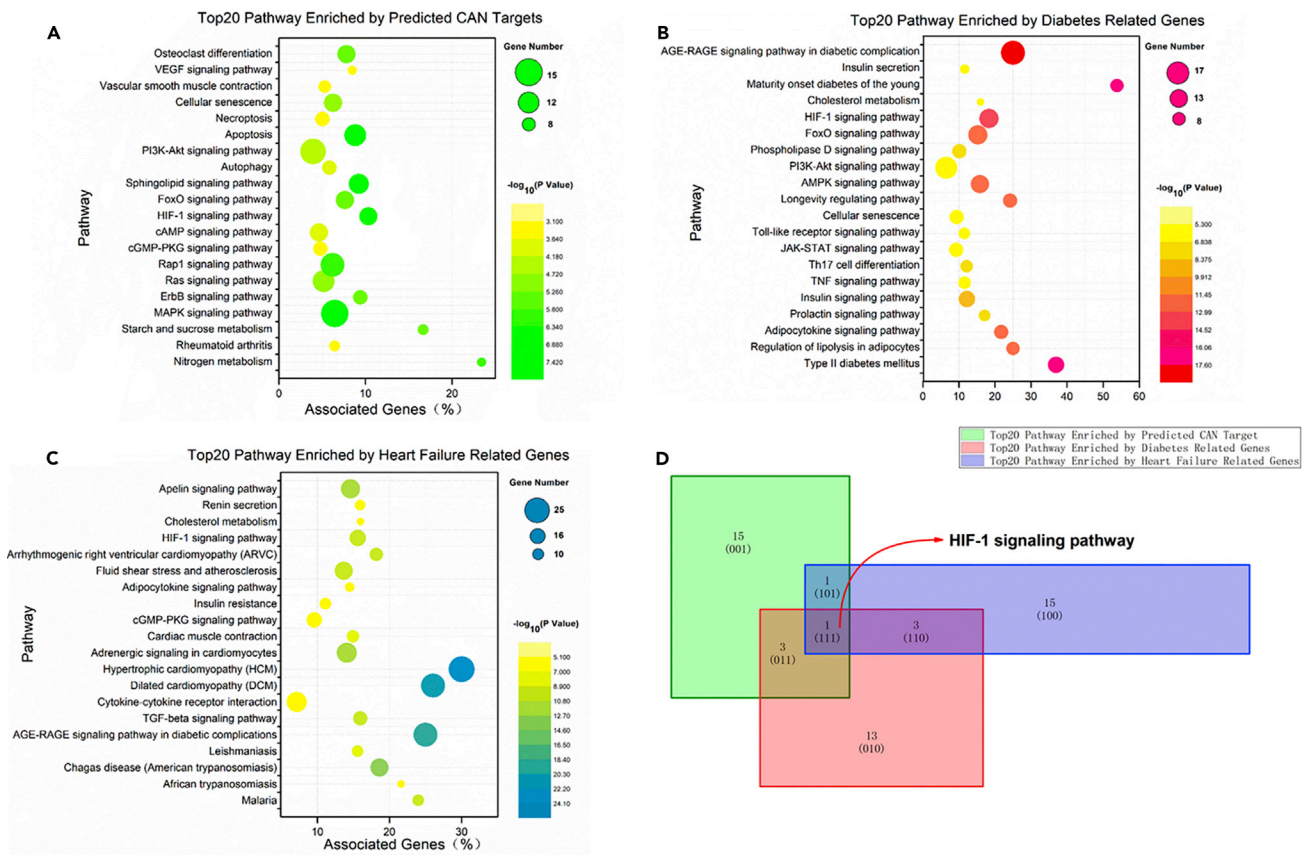
Figure 4. The enriched pathways of the predicated targets of CAN and diabetes- and HF-related genes

(A) The top 20 enriched pathways of the predicted targets of CAN, which were identified using CluoGo, p < 0.05.

(B) The top 20 enriched pathways of the diabetes-related genes (from the top 200 using GeneCards) using CluoGo, p < 0.001.

(C) The top 20 enriched pathways of the HF-related genes (from the top 200 using GeneCards) using CluoGo, p < 0.001.

(D) The common pathways of (A), (B), and (C) were analyzed using Origin 2018. HF, heart failure; CAN, canagliflozin.

indicated that CAN might inhibit mTOR phosphorylation by binding to the mTOR FRB domain, which is the same as with RAPA. Owing to the low expression level of the SGLT2 receptor in the hearts of humans and mice (Vrhovac et al., 2015), mTOR might be a new target of CAN in cardiovascular diseases, independent of the SGLT2 receptor.

mTOR and HIF-1α inhibitors are a potential strategy in heart lipotoxicity protection

Chronic activation of the mTOR and HIF-1 signaling pathway might mediate lipotoxicity in diabetic cardi-ocytes. LW6 is a specific HIF-1 inhibitor, which promotes the proteasomal degradation of wild-type HIF-1α by affecting HIF-1α protein stability (Lee et al., 2010). RAPA could inhibit mTOR phosphorylation and further inhibit the downstream HIF-1α transcription and protein expression level (Dodd et al., 2015; Naka-zawa et al., 2017; Mi et al., 2014). Next, we detected the cell survival protection and anti-inflammation ef-fects of the HIF-1α and mTOR inhibitors in the PA-induced HL-1 cell line to investigate the effects of HIF-1α on PA-induced inflammation and cellular toxicities. The results showed that RAPA and LW6 prevented cell death induced by PA (Figures 7A and 7F) and significantly reduced the mRNA expression level of *Il-1α*, *Il-6*, and *Tnf-α* (Figures 7B–7D and 7G–7I). LW6 did not significantly change the HIF-1α mRNA expression level (Figure 7E), but inhibited the HIF-1α protein function (Figures 7K and 7L) as previously reported (Lee et al., 2010). Similar to CAN, RAPA could significantly inhibit the increase of HIF-1α mRNA and protein expression levels induced by PA (Figures 7J–7L, see also Data S2). A previous study also found that RAPA exerted car-dioprotective effects on myocardial dysfunction during sepsis induced by cecal ligation and puncture in rats through the mTOR-HIF-1α axis and autophagy (Han et al., 2018). However, increasing research has found an association between high HIF-α expression level and inflammation and metabolic and
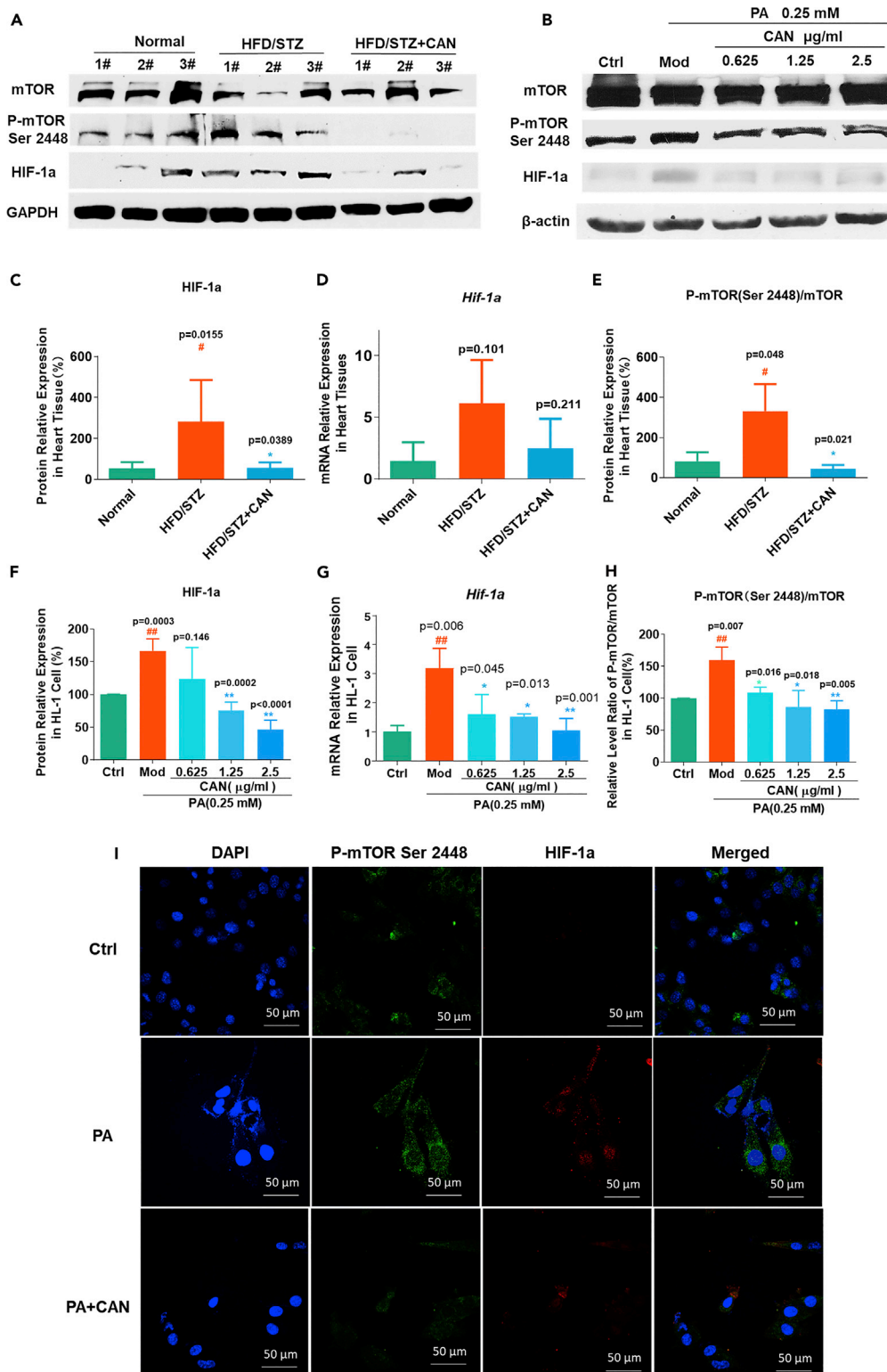
Figure 5. CAN inhibited the mTOR-HIF-1 signaling pathway *in vivo* and *in vitro*

(A–H) HIF-1a, p-mTOR (Ser 2448), and mTOR expression levels in (A) the hearts of the HFD/STZ-induced diabetic mice and in (B) the HL-1 cells were determined using western blot analysis. Relative expression level of (C) *Hif-1a* mRNA and quantification of (D) HIF-1α protein in the hearts of the HFD/STZ-induced diabetic mice was done using ImageJ software

Figure 5. Continued

following western blot analysis. Relative expression levels of (E) p-mTOR (Ser 2448)/mTOR protein expression ratio in the hearts of the HFD/STZ-induced diabetic mice was determined using ImageJ following western blot analysis. Relative expression level of (F) *Hif-1a* mRNA and the quantification of (G) HIF-1α protein in the HL-1 cells was done using RT-qPCR and ImageJ software following western blot analysis. Relative expression levels of (H) p-mTOR (Ser 2448)/mTOR protein expression ratio in the HL-1 cells was determined using ImageJ software following western blot analysis (H).

(I) Immunofluorescence analysis of the HL-1 cells using a confocal microscope (I). Magnification, ×600. Green fluorescence indicates p-mTOR (Ser 2448), red fluorescence indicates HIF-1α, blue fluorescence indicates DAPI, and merged indicates merged signal of p-mTOR (Ser 2448), HIF-1α, and DAPI. Data are presented as the mean ± SD. n = 5 or 3. #p < 0.05 and ##p < 0.01 versus normal or blank control; *p < 0.05 and **p < 0.01 versus HFD/STZ or PA. HFD, high-fat diet; STZ, streptozotocin; CAN, canagliflozin; normal, normal control group; HFD/STZ, HFD/STZ-induced diabetic control group; HFD/STZ + CAN, canagliflozin-treated HFD/STZ-induced diabetic group; PA, palmitic acid; Ctrl, untreated normal or blank control; Mod/PA, PA (0.25 mM)-treated control group; 0.625, HL-1 cells were treated with PA (0.25 mM) and CAN (0.625 μg/mL); 1.25, HL-1 cells were treated with PA (0.25 mM) and CAN (1.25 μg/mL); 2.5, HL-1 cells were treated with PA (0.25 mM) and CAN (2.5 μg/mL); PA + CAN, HL-1 cells treated with PA (0.25 mM) and CAN (2.5 μg/mL); p, phosphorylated.

cardiovascular disease, and the HIF-1α inhibitor was considered to be a potential therapeutic strategy (Majmundar et al., 2010). These results indicated that inhibition of the mTOR or HIF-1α signaling pathway could prevent lipotoxicity in the heart and serve as an important target. CAN might have similar pharmacological activities to these mTOR inhibitors.

DISCUSSION

Lipid metabolism provides the main energy source for heart function, but excessive lipid metabolism in the heart may affect heart function (Chen et al., 2018). In diabetes, impaired glucose and lipid metabolism and increased fat intake could lead to increased lipotoxicity in hearts and cause the development of diabetic cardiomyopathy or HF (Athithan et al., 2019). In this study, CAN significantly reduced blood glucose and lipid levels in the serum and hearts of diabetic mice. Also, we investigated the effects of CAN in livers of mice; we found that CAN significantly inhibited the increase of triglyceride and cholesterol levels in livers (Figure S1). Previous study indicated that CAN reduced serum insulin and increased insulin sensitivity and also promoted fat metabolism and regulated ketone levels after increasing urine glucose excretion (Tian et al., 2016; Yang et al., 2021; Kutoh and Hayashi, 2019). These effects of CAN may be useful to reduce systematic oxidative stress and inflammation in diabetic hearts. In addition, we investigated the effects of CAN in normal control mice and found that CAN slightly lowered body weight, blood glucose, and total cholesterol levels but did not significantly affect diet or water intake in normal mice (Figure S2). These results indicated that CAN affects glucose and lipid metabolism and then improves heart dysfunctions likely by targeting kidney SGLT2 and promoting urine glucose excretion. However, in another non-diabetic model, CAN did not affect glucose and lipid metabolism but still improved heart functions (Hasan et al., 2020). Our present result *in vitro* also indicated that CAN exerts a direct protective effect in cardiomyocytes independently of glucose and lipid metabolism. Collectively, these results indicated that CAN could exert cardioprotective effects in diabetic hearts likely in either an SGLT2-dependent or SGLT2-independent manner if it was used in diabetic patients. Most of hypoglycemic or hypolipidemic drugs did not show ideal cardioprotective effects at all in diabetic cardiomyopathy or HF, suggesting that diabetic cardiomyopathy or HF actually involves complicated pathological process beside glucose and lipid metabolism dysfunctions. The exact molecular mechanisms involved in pathological procession of diabetic cardiomyopathy or diabetic HF need to be further elucidated.

Diabetic cardiomyopathy was found to increase fat accumulation and oxidative metabolism, which causes an increased production of mitochondrial ROS (Kaludercic and Di Lisa, 2020; Palomer et al., 2013). Cardiomyocyte lipotoxicity is an important risk factor in diabetic cardiomyopathy development (Tong et al., 2019). Many dietary saturated fatty acids, such as PA, exist in numerous types of unhealthy food and induce lipid accumulation and lipotoxicity in the heart (Dalla Valle et al., 2019). Therefore, in this study, we used HFD, combined with STZ, to induce the animal model of diabetic cardiomyopathy in mice. Impaired glucose metabolism also led to lipid accumulation and FAO increase in diabetic hearts (Goldberg et al., 2012), and the increased FAO further promoted mitochondrial ROS generation. CAN inhibited energy metabolism by targeting mitochondrial complex 1 (Secker et al., 2018), in an off-target manner, which was independent of the SGLT2 receptor. In our previous studies, CAN significantly inhibited intracellular glucose metabolism (Xu et al., 2018; Zhong et al., 2020). These phenomena might partly explain why CAN inhibited ROS production, as observed in this study.
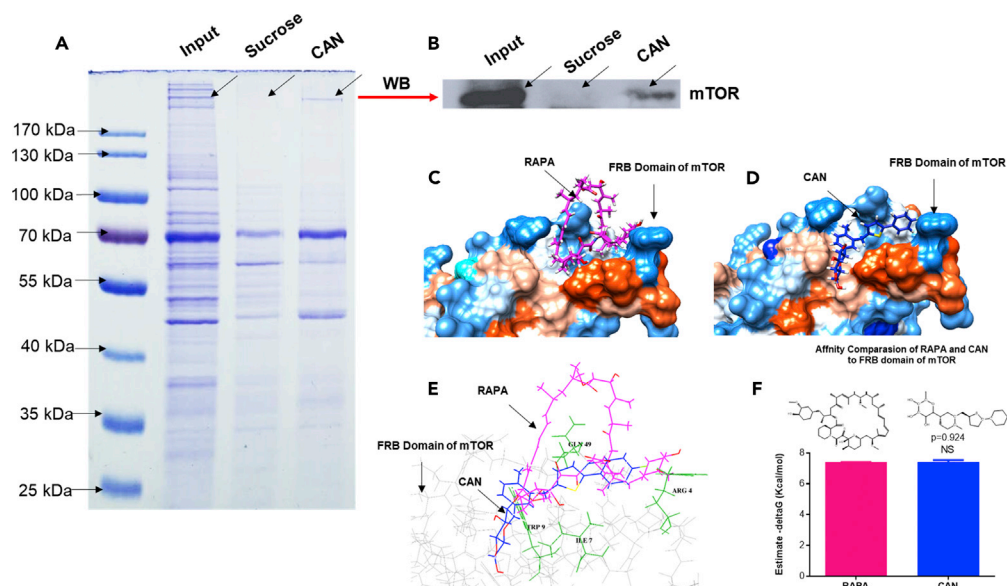
Figure 6. CAN inhibited mTOR phosphorylation by binding to the FRB domain within mTOR

(A) Affinity chromatography results of CAN.

(B–D) (B) Protein identified using western blot analysis in (A). Molecular docking of (C) RAPA and (D) CAN binding to the FRB domain within mTOR.

(E) Common binding site of the FRB domain within mTOR to RAPA and CAN.

(F) Comparison of the predicted Gibbs free energy of RAPA and CAN binding to the FRB domain of mTOR (n = 5). RAPA, rapamycin; CAN, canagliflozin; NS, no significant difference; FRB, FKBP-RAPA-binding.

Impaired glucose metabolism, increased lipid accumulation and ROS levels might cause hypoxia and chronic pathological expression level of HIF-1α in the heart (Warbrick and Rabkin, 2019; Movafagh et al., 2015). Chronic activation of HIF-1α was responsible for recruiting M1 macrophages in the heart and mediated metabolic inflammation in cardiomyocytes, thereby releasing IL-6, MCP-1, TNF-α, and IL-1β; NADPH oxidase; and connective tissue growth factor; the resulting chronic inflammation accelerated cardiac fibrosis and impaired the cardiac diastolic function (Warbrick and Rabkin, 2019) (Warbrick and Rabkin, 2019). Recently, research found that knock out of HIF-1α protected HF in the animal model (Kumar et al., 2018). As identified by the bioinformatics analysis, the HIF-1α signaling pathway could play an important role in the pathogenesis of diabetes and HF. The reduction in ROS generation by CAN might promote HIF-1α degradation, decrease the stability of HIF-1α, and inhibit the expression level of inflammatory factors induced by lipotoxicity.

mTOR serves as a central regulator of lipid storage and metabolism (Chakrabarti and Kandror, 2015). High-fat uptake promoted mTOR phosphorylation (Kling et al., 2018). Following mTOR activation, the accumulation of triglycerides is facilitated by the increase in adipogenesis and lipogenesis (Caron et al., 2015), which also contributed to lipotoxicity. The inhibition of mTOR has been hypothesized to have beneficial effects against atherosclerosis, cardiac hypertrophy, and HF (Sanches-Silva et al., 2020). Furthermore, mTOR could directly activate HIF-1α transcription and upregulate the HIF-1α protein expression level, and conversely, the inhibition of mTOR by RAPA attenuated the HIF-1α expression level (Chen et al., 2012). Therefore, a promising strategy in the treatment of HF induced by lipotoxicity is to target the mTOR/HIF-1α axis. In this study, we proved that RAPA (mTOR inhibitor) and LW6 (HIF-1α inhibitor) exerted significant anti-inflammatory activities in the PA-induced HL-l cell line. This result indicated that the mTOR/HIF-1α mediator could alleviate the development of cardiomyocyte inflammation and cell toxicities induced by lipid overload. Compared with that in the mTOR and HIF-1α inhibitors, CAN could inhibit mTOR phosphorylation and HIF-1α transcription and expression, similar to RAPA.

Furthermore, we used molecular docking and affinity chromatography methods to confirm that CAN had a direct molecular interaction with the FRB domain of mTOR and might be a new inhibitor of mTOR phosphorylation. However, in our preliminary study, this activity of CAN seemed not to be specific to CAN itself
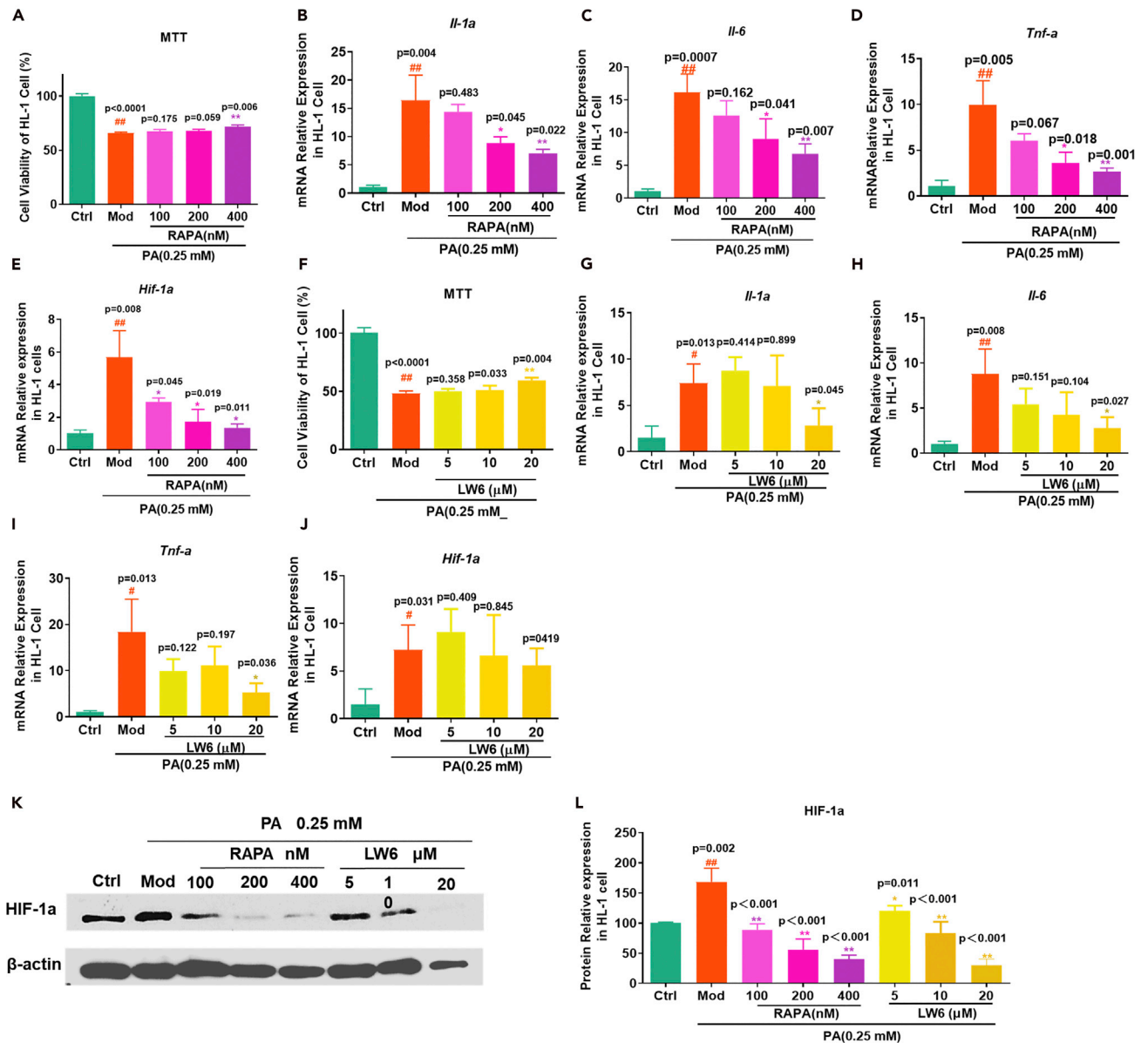
Figure 7. Protective effects of the mTOR inhibitor, RAPA, and the HIF-1a inhibitor LW6 on PA-induced HL-1 cell viability and inflammation

(A–E) (A) Cell viability was detected using an MTT assay in the RAPA-treated HL-1 cells (n = 3). mRNA expression levels of (B) *Il-1a*, (C) *Il-6*, (D) *Tnf-a*, and (E) *Hif-1a* in the RAPA-treated HL-1 cells (n = 3).

(F–J) (F) Cell viability was detected using an MTT assay in the LW6-treated HL-1 cells (n = 3). mRNA expression levels of (G) *Il-1a*, (H) *Il-6*, (I) *Tnf-a*, and (J) *Hif-1a* in the LW6-treated HL-1 cells (n = 3).

(K and L) (L) Protein expression levels of HIF-1a in RAPA and LW6-treated HL-1cells was determined using ImageJ software following western blot analysis (K). Data are presented as mean $\pm$ SD. [#]p < 0.05 and [##]p < 0.01 versus ctrl; *p < 0.05 and **p < 0.01 versus Mod. Ctrl, untreated normal control; Mod, PA (0.25 mM)-treated control group; 100, HL-1 cells were treated with PA (0.25 mM) and RAPA (100 nM); 200, HL-1 cells were treated with PA (0.25 mM) and RAPA (200 nM); 400, HL-1 cells were treated with PA (0.25 mM) and RAPA (400 nM); 5, HL-1 cells were treated with PA (0.25 mM) and LW6 (5 µM); 10, HL-1 cells were treated with PA (0.25 mM) and LW6 (10 µM); 20, HL-1 cells were treated with PA (0.25 mM) and LW6 (20 µM).

because other SGLT2 inhibitors, e.g., dapagliflozin or empagliflozin, showed similar physical interaction of CAN with mTOR (Figures S3 and S4, see also Data S1). Further physical interaction and activity evaluation should be investigated about these SGLT2 inhibitors and their potential target mTOR. In addition, although we had confirmed that mTOR could be a key target of CAN, other key factors in PI3K-AKT pathway
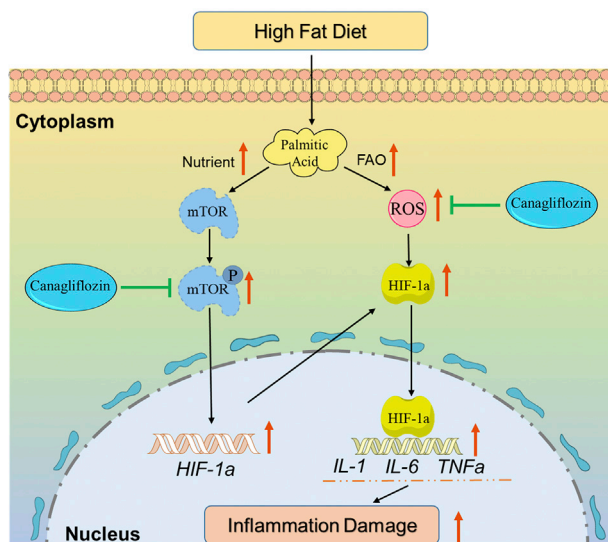
Figure 8. Protective mechanisms of canagliflozin on lipotoxicity or inflammatory damage induced by palmitic acid in cardiomyocytes

FAO, fatty acid oxidation; ROS, reactive oxygen species.

also were predicated as the targets of CAN through molecular docking. Whether CAN also affects mTOR activity by PI3K-AKT pathway remains a matter further investigation because mTOR can be regulated by PI3K-AKT pathway (Magaye et al., 2021). Actually, CAN activated AKT in the previous study (Song et al., 2020). Collectively, CAN might affect mTOR activity in a direct or indirect manner. However, more exact mechanisms should be investigated in the future.

In summary, we confirmed the protective effects of CAN on lipotoxicity, e.g., oxidative stress, inflammation, and cellular toxicities in the hearts of the diabetic C57BL/6 mouse models induced by HFD/STZ and in the PA-treated HL-1 cell line. The molecular mechanisms of CAN might be mediated by directly binding to the mTOR protein and inhibiting mTOR phosphorylation and then inhibiting HIF-1α mRNA and protein expression levels (Figure 8). This research indicated that the mTOR/HIF-1α signaling pathway could be involved in lipotoxicity in cardiomyocytes. Furthermore, CAN might exert protective effects on lipotoxicity in diabetic hearts as diabetic hearts are usually associated with increased lipid metabolism dysfunction. However, further validation *in vivo* should be conducted in the future. These results may partly explain why CAN significantly reduced the number of HF events in diabetic patients and provide a promising target in the development of a new drug against diabetic HF. The SGLT2 inhibitor might have a new drug target by targeting the mTOR/HIF-1α pathway in the cardiovascular system, which is independent of the kidney SGLT2 receptor.

Limitations of the study

This study has some limitations. First, how CAN is taken up by cells and directly binds to mTOR to suppress its function and whether mTOR is the specific target of CAN in diabetic HF treatment are not involved in this research and need further investigation. Second, the exact molecular docking mechanism e.g., the binding sites between CAN and the amino acids of the mTOR protein, requires further identification in the future.

STAR★METHODS

Detailed methods are provided in the online version of this paper and include the following:

- KEY RESOURCES TABLE
- RESOURCE AVAILABILITY
  - Lead contact
  - Materials availability
  - Data and code availability

Table 1. Primers for mRNA qPCR

Gene	Forward	Reverse	NCBI	Size
Hif-1α (mouse)	ACCTTCATCGGAAAC TCCAAAG	ACTGTTAGGCTCAGG TGAACT	NM_001313919.1	156
Il-1α (mouse)	TCTGCCATTGACCATC TC	ATCTTCCCGTTGCTTG AC	NM_010554.4	182
Il-6 (mouse)	CTGCAAGAGACTTCC ATCCAG	GAGTGGTATAGACAG GTCTGTTGG	NM_031168	131
Tnf-α (mouse)	GGGCTTCCAGAACTC CA	GCTACAGGCTTGTCAC TCG	NM_013693.2	213
β-Actin (mouse)	GTGACGTTGACATCC GTAAAGA	GCCGGACTCATCGTAC TCC	NM_007393	245

- EXPERIMENTAL MODEL AND SUBJECT DETAILS
  - HFD/STZ-induced diabetic mouse models
  - Cell culture
- METHOD DETAILS
  - Biochemical analysis in animals
- MTT ASSAY
  - RT-qPCR assay
  - Western blot analysis
  - ROS assay
  - Immunofluorescence and confocal assay
  - Apoptosis assays
  - Pathway enrichment analysis
  - Molecular docking assay
  - Affinity chromatography
- QUANTIFICATION AND STATISTICAL ANALYSIS

AUTHOR CONTRIBUTIONS

P.S. contributed to investigation, data curation, data analysis, and manuscript writing; Y.W. and Y.D. contributed to investigation and data validation; J.L. and J.Z. contributed to investigation; Y.Z. and N.X. contributed to manuscript revision; W.X. contributed to project administration, supervision, conceptualization, data analysis, and manuscript writing and revision.

DECLARATION OF INTERESTS

The authors declare no competing interests.

REFERENCES

Abe, H., Semba, H., and Takeda, N. (2017). The roles of hypoxia signaling in the pathogenesis of cardiovascular diseases. J. Atheroscler. Thromb. *24*, 884–894.

Aimo, A., Castiglione, V., Borrelli, C., Saccaro, L.F., Franzini, M., Masi, S., Emdin, M., and Giannoni, A. (2020). Oxidative stress and inflammation in the evolution of heart failure: from pathophysiology to therapeutic strategies. Eur. J. Prev. Cardiol. *27*, 494–510.

Athithan, L., Gulsin, G.S., McCann, G.P., and Levelt, E. (2019). Diabetic cardiomyopathy: pathophysiology, theories and evidence to date. World J. Diabetes *10*, 490–510.

Bindea, G., Mlecnik, B., Hackl, H., Charoentong, P., Tosolini, M., Kirilovsky, A., Fridman, W.H., Pages, F., Trajanoski, Z., and Galon, J. (2009). ClueGO: a Cytoscape plug-in to decipher functionally grouped gene ontology and pathway annotation networks. Bioinformatics *25*, 1091–1093.

Bugger, H., and Abel, E.D. (2014). Molecular mechanisms of diabetic cardiomyopathy. Diabetologia *57*, 660–671.

Caron, A., Richard, D., and Laplante, M. (2015). The roles of mTOR complexes in lipid metabolism. Annu. Rev. Nutr. *35*, 321–348.

Chakrabarti, P., and Kandror, K.V. (2015). The role of mTOR in lipid homeostasis and diabetes progression. Curr. Opin. Endocrinol. Diabetes Obes. *22*, 340–346.

Chen, H., Xiong, T., Qu, Y., Zhao, F., Ferriero, D., and Mu, D. (2012). mTOR activates hypoxia-inducible factor-1α and inhibits neuronal apoptosis in the developing rat brain during the early phase after hypoxia-ischemia. Neurosci. Lett. *507*, 118–123.

Chen, D., Li, X., Zhang, L., and Gao, L. (2018). A high-fat diet impairs mitochondrial biogenesis, mitochondrial dynamics, and the respiratory chain complex in rat myocardial tissues. J. Cell. Biochem. *119*, 9602.

Chen, F., Zhu, K., Chen, L., Ouyang, L., Chen, C., Gu, L., Jiang, Y., Wang, Z., Lin, Z., Zhang, Q., et al. (2020). Protein target identification of ginsenosides in skeletal muscle tissues: discovery of natural small-molecule activators of muscle-type creatine kinase. J. Ginseng Res. *44*, 461–474.

Cui, K., Zhang, S., Jiang, X., and Xie, W. (2016). Novel synergic antidiabetic effects of Astragalus polysaccharides combined with Crataegus flavonoids via improvement of islet function and liver metabolism. Mol. Med. Rep. *13*, 4737–4744.

Daina, A., Michielin, O., and Zoete, V. (2019). SwissTargetPrediction: updated data and new features for efficient prediction of protein targets of small molecules. Nucleic Acids Res. *47*, W357–W364.

Dalla Valle, A., Vertongen, P., Spruyt, D., Lechanteur, J., Suain, V., Gaspard, N., Brion, J.P., Gangji, V., and Rasschaert, J. (2019). Induction of stearoyl-CoA 9-desaturase 1 protects human mesenchymal stromal cells against palmitic acid-induced lipotoxicity and inflammation. Front. Endocrinol. *10*, 726.

Dodd, K.M., Yang, J., Shen, M.H., Sampson, J.R., and Tee, A.R. (2015). mTORC1 drives HIF-1alpha and VEGF-A signalling via multiple mechanisms involving 4E-BP1, S6K1 and STAT3. Oncogene *34*, 2239–2250.

Fillmore, N., Mori, J., and Lopaschuk, G.D. (2014). Mitochondrial fatty acid oxidation alterations in heart failure, ischaemic heart disease and diabetic cardiomyopathy. Br. J. Pharmacol. *171*, 2080–2090.

Goldberg, I.J., Trent, C.M., and Schulze, P.C. (2012). Lipid metabolism and toxicity in the heart. Cell Metab. *15*, 805–812.

Grosdidier, A., Zoete, V., and Michielin, O. (2011). SwissDock, a protein-small molecule docking web service based on EADock DSS. Nucleic Acids Res. *39*, W270–W277.

Han, W., Wang, H., Su, L., Long, Y., Cui, N., and Liu, D. (2018). Inhibition of the mTOR pathway exerts cardioprotective effects partly through autophagy in CLP rats. Mediators Inflamm. *2018*, 4798209.

Hasan, R., Lasker, S., Hasan, A., Zerin, F., Zamila, M., Chowdhury, F.I., Nayan, S.I., Rahman, M.M., Khan, F., Subhan, N., et al. (2020). Canagliflozin attenuates isoprenaline-induced cardiac oxidative stress by stimulating multiple antioxidant and anti-inflammatory signaling pathways. Sci. Rep. *10*, 14459.

Heintjes, E.M., Houben, E., Beekman-Hendriks, W.L., Lighaam, E., Cremers, S.M., Penning-Van Beest, F.J.A., Stehouwer, C.D.A., and Herings, R.M.C. (2019). Trends in mortality, cardiovascular complications, and risk factors in type 2 diabetes. Neth. J. Med. *77*, 317–329.

Inoue, M., Hayashi, A., Taguchi, T., Arai, R., Sasaki, S., Takano, K., Inoue, Y., and Shichiri, M. (2019). Effects of canagliflozin on body composition and hepatic fat content in type 2 diabetes patients with non-alcoholic fatty liver disease. J. Diabetes Investig. *10*, 1004–1011.

Jones, D.P., and Patel, J. (2018). Therapeutic approaches targeting inflammation in cardiovascular disorders. Biology (Basel) *7*, 49.

Kaludercic, N., and Di Lisa, F. (2020). Mitochondrial ROS formation in the pathogenesis of diabetic cardiomyopathy. Front. Cardiovasc. Med. *7*, 12.

Kling, D.N., DeBose-Scarlett, E.M., Teixeira, L.D., Gezan, S.A., Lorca, G.L., and Gonzalez, C.F. (2018). Sex modulates lactobacillus johnsonii N6.2 and phytophenol effectiveness in reducing high fat diet induced mTOR activation in sprague-dawley rats. Front. Microbiol. *9*, 2649.

Kumar, S., Wang, G., Liu, W., Ding, W., Dong, M., Zheng, N., Ye, H., and Liu, J. (2018). Hypoxia-induced mitogenic factor promotes cardiac hypertrophy via calcium-dependent and hypoxia-inducible factor-1alpha mechanisms. Hypertension *72*, 331–342.

Kutoh, E., and Hayashi, J. (2019). Effect of canagliflozin on heart function involving ketone bodies in patients with type 2 diabetes. Drug Res. (Stuttg) *69*, 297–300.

Land, S.C., and Tee, A.R. (2007). Hypoxia-inducible factor 1alpha is regulated by the mammalian target of rapamycin (mTOR) via an mTOR signaling motif. J. Biol. Chem. *282*, 20534–20543.

Lee, K., Kang, J.E., Park, S.K., Jin, Y., Chung, K.S., Kim, H.M., Lee, K., Kang, M.R., Lee, M.K., Song, K.B., et al. (2010). LW6, a novel HIF-1 inhibitor, promotes proteasomal degradation of HIF-1alpha via upregulation of VHL in a colon cancer cell line. Biochem. Pharmacol. *80*, 982–989.

Lim, V.G., Bell, R.M., Arjun, S., Kolatsi-Joannou, M., Long, D.A., and Yellon, D.M. (2019). SGLT2 inhibitor, canagliflozin, attenuates myocardial infarction in the diabetic and nondiabetic heart. JACC Basic Transl. Sci. *4*, 15–26.

Liu, Q., Wang, S., and Cai, L. (2014). Diabetic cardiomyopathy and its mechanisms: role of oxidative stress and damage. J. Diabetes Investig. *5*, 623–634.

Lopaschuk, G.D., Belke, D.D., Gamble, J., Itoi, T., and Schonekess, B.O. (1994). Regulation of fatty acid oxidation in the mammalian heart in health and disease. Biochim. Biophys. Acta *1213*, 263–276.

Magaye, R.R., Savira, F., Hua, Y., Xiong, X., Huang, L., Reid, C., Flynn, B.L., Kaye, D., Liew, D., and Wang, B.H. (2021). Attenuating PI3K/Akt-mTOR pathway reduces dihydrosphingosine 1 phosphate mediated collagen synthesis and hypertrophy in primary cardiac cells. Int. J. Biochem. Cell Biol. *134*, 105952.

Majmundar, A.J., Wong, W.J., and Simon, M.C. (2010). Hypoxia-inducible factors and the response to hypoxic stress. Mol. Cell *40*, 294–309.

Mangali, S., Bhat, A., Udumula, M.P., Dhar, I., Sriram, D., and Dhar, A. (2019). Inhibition of protein kinase R protects against palmitic acid-induced inflammation, oxidative stress, and apoptosis through the JNK/NF-kB/NLRP3 pathway in cultured H9C2 cardiomyocytes. J. Cell. Biochem. *120*, 3651–3663.

Marz, A.M., Fabian, A.K., Kozany, C., Bracher, A., and Hausch, F. (2013). Large FK506-binding proteins shape the pharmacology of rapamycin. Mol. Cell. Biol. *33*, 1357–1367.

Mi, C., Ma, J., Shi, H., Li, J., Wang, F., Lee, J.J., and Jin, X. (2014). 4',6-dihydroxy-4-methoxyisoaurone inhibits the HIF-1alpha pathway through inhibition of Akt/mTOR/p70S6K/4E-BP1 phosphorylation. J. Pharmacol. Sci. *125*, 193–201.

Movafagh, S., Crook, S., and Vo, K. (2015). Regulation of hypoxia-inducible factor-1a by reactive oxygen species: new developments in an old debate. J. Cell. Biochem. *116*, 696–703.

Nakazawa, H., Ikeda, K., Shinozaki, S., Kobayashi, M., Ikegami, Y., Fu, M., Nakamura, T., Yasuhara, S., Yu, Y.M., Martyn, J.A.J., et al. (2017). Burn-induced muscle metabolic derangements and mitochondrial dysfunction are associated with activation of HIF-1alpha and mTORC1: role of protein farnesylation. Sci. Rep. *7*, 6618.

Nalban, N., Sangaraju, R., Alavala, S., Mir, S.M., Jerald, M.K., and Sistla, R. (2020). Arbutin

attenuates isoproterenol-induced cardiac hypertrophy by inhibiting TLR-4/NF-κB pathway in mice. Cardiovasc. Toxicol. *20*, 235–248.

O'Grady, H., Mostafa, K., Zafar, H., Lohan, D., Morris, L., and Sharif, F. (2019). Changes in left ventricular shape and morphology in the presence of heart failure: a four-dimensional quantitative and qualitative analysis. Int. J. Comput. Assist. Radiol. Surg. *14*, 1415–1430.

Palomer, X., Salvadó, L., Barroso, E., and Vázquez-Carrera, M. (2013). An overview of the crosstalk between inflammatory processes and metabolic dysregulation during diabetic cardiomyopathy. Int. J. Cardiol. *168*, 3160–3172.

Pettersen, E.F., Goddard, T.D., Huang, C.C., Couch, G.S., Greenblatt, D.M., Meng, E.C., and Ferrin, T.E. (2004). UCSF Chimera–a visualization system for exploratory research and analysis. J. Comput. Chem. *25*, 1605–1612.

Rådholm, K., Figtree, G., Perkovic, V., Solomon, S.D., Mahaffey, K.W., De Zeeuw, D., Fulcher, G., Barrett, T.D., Shaw, W., Desai, M., et al. (2018). Canagliflozin and heart failure in type 2 diabetes mellitus: results from the CANVAS program. Circulation *138*, 458–468.

Rana, J.S., Nieuwdorp, M., Jukema, J.W., and Kastelein, J.J. (2007). Cardiovascular metabolic syndrome - an interplay of, obesity, inflammation, diabetes and coronary heart disease. Diabetes Obes. Metab. *9*, 218–232.

Rijzewijk, L.J., van der Meer, R.W., Smit, J.W., Diamant, M., Bax, J.J., Hammer, S., Romijn, J.A., De Roos, A., and Lamb, H.J. (2008). Myocardial steatosis is an independent predictor of diastolic dysfunction in type 2 diabetes mellitus. J. Am. Coll. Cardiol. *52*, 1793–1799.

Sanches-Silva, A., Testai, L., Nabavi, S.F., Battino, M., Pandima Devi, K., Tejada, S., Sureda, A., Xu, S., Yousefi, B., Majidinia, M., et al. (2020). Therapeutic potential of polyphenols in cardiovascular diseases: regulation of mTOR signaling pathway. Pharmacol. Res. *152*, 104626.

Secker, P.F., Beneke, S., Schlichenmaier, N., Delp, J., Gutbier, S., Leist, M., and Dietrich, D.R. (2018). Canagliflozin mediated dual inhibition of mitochondrial glutamate dehydrogenase and complex I: an off-target adverse effect. Cell Death Dis. *9*, 226.

Song, Z., Zhu, J., Wei, Q., Dong, G., and Dong, Z. (2020). Canagliflozin reduces cisplatin uptake and activates Akt to protect against cisplatin-induced nephrotoxicity. Am. J. Physiol. Ren. Physiol *318*, F1041–F1052.

Tian, C.M., Jiang, X., Ouyang, X.X., Zhang, Y.O., and Xie, W.D. (2016). Berberine enhances antidiabetic effects and attenuates untoward effects of canagliflozin in streptozotocin-induced diabetic mice. Chin. J. Nat. Med. *14*, 518–526.

Tong, M., Saito, T., Zhai, P., Oka, S.I., Mizushima, W., Nakamura, M., Ikeda, S., Shirakabe, A., and Sadoshima, J. (2019). Mitophagy is essential for maintaining cardiac function during high fat diet-induced diabetic cardiomyopathy. Circ. Res. *124*, 1360–1371.

Vrhovac, I., Balen Eror, D., Klessen, D., Burger, C., Breljak, D., Kraus, O., Radovic, N., Jadrijevic, S., Aleksic, I., Walles, T., et al. (2015). Localizations of Na(+)-D-glucose cotransporters SGLT1 and SGLT2 in human kidney and of SGLT1 in human small intestine, liver, lung, and heart. Pflugers Arch. *467*, 1881–1898.

Warbrick, I., and Rabkin, S.W. (2019). Hypoxia-inducible factor 1-alpha (HIF-1alpha) as a factor mediating the relationship between obesity and heart failure with preserved ejection fraction. Obes. Rev. *20*, 701–712.

Xie, W., Nie, Y., Du, L., Zhang, Y., and Cai, G. (2007). Preventive effects of fenofibrate on insulin resistance, hyperglycaemia, visceral fat accumulation in NIH mice induced by small-dose streptozotocin and lard. Pharmacol. Res. *55*, 392–399.

Xu, C., Wang, W., Zhong, J., Lei, F., Xu, N., Zhang, Y., and Xie, W. (2018). Canagliflozin exerts anti-inflammatory effects by inhibiting intracellular glucose metabolism and promoting autophagy in immune cells. Biochem. Pharmacol. *152*, 45–59.

Yang, X., Liu, Q., Li, Y., Ding, Y., Zhao, Y., Tang, Q., Wu, T., Chen, L., Pu, S., Cheng, S., et al. (2021). Inhibition of the sodium-glucose co-transporter SGLT2 by canagliflozin ameliorates diet-induced obesity by increasing intra-adipose sympathetic innervation. Br. J. Pharmacol. *178*, 1756–1771.

Zhang, Y., Bauersachs, J., and Langer, H.F. (2017). Immune mechanisms in heart failure. Eur. J. Heart Fail. *19*, 1379–1389.

Zhong, J., Sun, P., Xu, N., Liao, M., Xu, C., Ding, Y., Cai, J., Zhang, Y., and Xie, W. (2020). Canagliflozin inhibits p-gp function and early autophagy and improves the sensitivity to the antitumor effect of doxorubicin. Biochem. Pharmacol. *175*, 113856.

STAR★METHODS

KEY RESOURCES TABLE

REAGENT or RESOURCE	SOURCE	IDENTIFIER
Antibodies		
mTOR (7C10) Rabbit mAb	Cell Signaling Technology,USA	Cat#2983;RRID: AB_2105622
Phospho-mTOR (Ser2448) (D9C2) XP® Rabbit mAb	Cell Signaling Technology,USA	Cat#5536; RRID: AB_10691552
HIF-1α (D2U3T) Rabbit mAb	Cell Signaling Technology,USA	Cat#14179; RRID: AB_2622225
Anti-β-Actin antibody, Mouse monoclonal	Sigma-Aldrich,USA	Cat#A1978; RRID: AB_476692
Chemicals, peptides, and recombinant proteins		
Canagliflozin	Biochempartner, Shanghai, China	Cat# BCP38512
Rapamycin	MedChemExpress,USA	Cat#HY-10219
LW6	MedChemExpress,USA	Cat# HY-13671
Palmitic Acid	Sigma-Aldrich,USA	P0500-10G
Critical commercial assays		
Evo M-MLV RT Premix RT-PCR kit	Accurate Biotechnology,Hunan,China	AG11728
SYBR Green Premix Pro Taq HS qPCR kit	Accurate Biotechnology,Hunan,China	AG11721
BNP Elisa Kit	YingxinBio,Shanghai,China	TX20633
LDH test reagent(kit)	BioSino,Beijing,China	E-BC-K044-S
Deposited data		
mTOR FRB domain Structure	PDB	PDB:4DRI
Canagliflozin Structure	Drugbank	https://go.drugbank.com/drugs/DB08907
Dapagliflozin Structure	DrugBank	https://go.drugbank.com/drugs/DB06292
Empagliflozin Structure	DrugBank	https://go.drugbank.com/drugs/DB09038
Rapamycin Structure	Drugbank	https://go.drugbank.com/drugs/DB00877
Heart Failure Related Gene	GeneCards	https://www.genecards.org/Search/Keyword?queryString=heart%20failure
Diabetes Related Gene	GeneCards	https://www.genecards.org/Search/Keyword?queryString=diabetes
Experimental models: Cell lines		
HL-1 Cell	Fenghui Bio,Hunan,China	CL0683
Experimental models: Organisms/strains		
C57/BL6J Mice	Guangdong Medical Laboratory Animal Center	NO.44007200081314
High Fat Diets	Beijing HFK Bioscience, Beijing,Chima	H10141
Oligonucleotides		
Primers for HIF-1a/IL-1a/IL6/TNF-a	This Paper	See Table 1
Software and algorithms		
Cytoscape	(Bindea et al., 2009)	https://cytoscape.org/

(Continued on next page)

Continued

REAGENT or RESOURCE	SOURCE	IDENTIFIER
Chimera 1.14	(Pettersen et al., 2004)	http://www.cgl.ucsf.edu/chimera/download.html
Swiss Target Prediction	(Daina et al., 2019)	http://www.swisstargetprediction.ch/
SwissDock	(Grosdidier et al., 2011)	http://www.swissdock.ch/

RESOURCE AVAILABILITY

Lead contact

Further information, requests, and raw data should be directed to and will be fulfilled by the lead contact Professor Weidong Xie (xiewd@sz.tsinghua.edu.cn).

Materials availability

Requests for further information or materials should be directed to the lead contact.

Data and code availability

Requests for biological datasets should be directed to the lead contact.

EXPERIMENTAL MODEL AND SUBJECT DETAILS

HFD/STZ-induced diabetic mouse models

C57BL/6J mice (body weight, 18±2 g; 4-weeks-old; male) were purchased from Guangzhou Medical Animal Centre (Guangzhou, China) and housed under controlled conditions (constant temperature: 22±2°C; constant humidity: 60±5%; 12 h dark/light cycle). The study was performed in strict accordance with the National Institutes of Health Guide for the Care and Use of Laboratory Animals and the protocol was approved by the Bioethics Committee of Shenzhen International Graduate School, Tsinghua University, China (Ethics issue [2020] No. 9). The diabetic mouse models were fed with HFD (41% energy from fat; Beijing HFK Bioscience, Beijing, China, H10141). The model group and drug treated group were intraperitoneally injected with STZ (40 mg/kg once before drug administration; Sangon Biotech Co., Ltd., Shanghai, China), which was freshly dissolved in ice-cold 0.1 M citrate solution (pH 4.5), according to a previous study (Xie et al., 2007). After one week, the diabetic mice with fasting blood glucose more than 11.1 mmol/L were divided into two groups: An untreated HFD/STZ control group and a CAN (Biochempartner, Shanghai, China)-treated group (25 mg/kg/d; dissolved in 0.5% sodium salt of carboxymethyl cellulose [CMC-Na; Sangon Biotech, Shanghai, China]). The intragastric dose of CAN administered to the mice was converted according to the clinical dose in humans (100 mg/kg/day). The normal control and HFD/STZ control groups were orally administered with an equal volume of 0.5% CMC-Na daily, CAN group were normal mice only treated with CAN (25 mg/kg/day) alone. The body weight of the mice, and food and water uptake were monitored once a week. After 12 weeks of treatment, the heart function was assayed by echocardiographic method. Briefly, the mice were subjected to an anesthesia with isopentane. Then, the left ventricular ejection fraction (LVEF) and left ventricular diastolic internal diameter (LVID) was analyzed by high-resolution small animal imaging system (Vevo 2100, VisualSonics, Toronto, Canada) equipped with 22–55 MHz transducer at a frame rate of 233 Hz. Finally, the mice were subjected to fasting for 6 h, anesthetized with urethane, which was dissolved in saline (intraperitoneal injection of urethane at a dose of 1000 mg kg-1; Sangon Biotech Co., Ltd., Shanghai, China), then sacrificed while under anesthesia. The blood was collected from the orbital plexus veins, and the serum was extracted from the blood samples using centrifugation (1000 rpm for 10 min at 4°C) and stored at -20°C for further analysis. Simultaneously, unrecovered anesthetized animals were sacrificed using cervical dislocation by skillful well-trained investigators, and the hearts, abdominal adipose tissues and livers were removed and weighed. A portion of the heart tissue was immersed in 4% paraformaldehyde solution for regular pathological slicing, and hematoxylin and eosin (H&E), wheat germ agglutinin (WGA) and Masson staining. The remaining samples were instantly frozen by using liquid nitrogen and stored at -80°C for further analysis.

Cell culture

The HL-1 cells were purchased from Fenghui Biotechnology Company, (Changsha, China) and cultured in high glucose DMEM (Gibco®; Thermo Fisher Scientific, Inc., USA) supplemented with 10% premium fetal bovine serum (Pan Biotech, Germany) and 1% penicillin-streptomycin antibiotic (Gibco™; Thermo Fisher Scientific, Inc., USA), at 37°C in a humidified atmosphere with 5% O_2. The cells were seeded at a density of either 8×10^3 cells per well in 96-well plates, 2×10^4 cells per well in 24-well plates, or 3×10^5 cells in 6-well plates (all from Guangzhou Jet Bio-Filtration Co., Ltd.). The HL-1 cells were incubated with PA (0.25 mM; Sigma-Aldrich, USA) for 24 h. Different concentrations of CAN (0.625, 1.25 and 2.5 μg/ml; Bio-chempartner, Shanghai,China), rapamycin (RAPA; 100, 200, and 400 nM; MedChemExpress, USA), and LW6 (5, 10 and 20 μM; MedChemExpress, USA) were added to investigate the anti-inflammatory activities on PA-induced HL-1 cell. PA was dissolved in 3% bovine serum albumin (BSA; Biofroxx, Germany) solution. CAN, RAPA, and LW6 were dissolved in dimethyl sulfoxide (DMSO; Beyotime Institute of Biotechnology, Shanghai, China). Blank control cells were treated with an equal volume of BSA or DMSO solution, the final concentration of DMSO in cell medium was 0.1%. After 24 h of treatment, oil red O (Sangon Biotech Co., Ltd., Shanghai, China) and WGA (Sigma-Aldrich, USA) staining was performed to observe fat accumulation and cell size, respectively. Total protein and RNA was extracted, as described previously (Xu C. et al., 2018). The mRNA expression levels of *Hif-1α*, *Il-1α*, *Il-6*, and *Tnf-α* were analyzed using reverse transcription-quantitative PCR (RT-qPCR). The phosphorylation of HIF-1α and mTOR was measured using western blot analysis.

METHOD DETAILS
Biochemical analysis in animals

The levels of serum cholesterol, triglyceride, glucose, lactate dehydrogenase (LDH) and creatine kinase (CK) were measured using regular commercial kits (BioSino Bio-Technology & Science Inc, Beijing, China). B-type natriuretic peptide (BNP) was detected using an ELISA kit (YingXinBio, Shanghai, China). Total protein from the heart tissue was extracted using a cell lysis buffer, and the protein concentration was determined with a commercial kit (both from Beyotime Institute of Biotechnology, Shanghai, China). The cholesterol, triglyceride, and glycogen levels in the heart tissues and liver were analyzed with commercial kits (Nanjing Jiancheng, Nanjing, China) and their levels were normalized to the protein concentration.

MTT ASSAY

MTT (Sangon Biotech, Shanghai, China) was dissolved in phosphate buffer solution (PBS; 0.01 M; pH,7.0) at a concentration of 5 mg/ml and sterilized by filtration with 0.22 μm filters. The HL-1 cells (8×10^3 per well) were seeded into 96-well plates. The CAN, RAPA and LW6 reagents were dissolved in DMSO. The HL-1 cells were incubated with PA (0.25 mM) for 24 h to induce lipotoxicity. Different concentrations of CAN (0.625, 1.25 and 2.5 μg/ml), RAPA (100, 200 and 400 nM), and LW6 (5, 10 and 20 μM) were simultaneously added for 24 h to investigate the protective activity on PA-induced lipotoxicity. The blank or untreated control groups were treated with an equal volume of BSA solution. After 24 h of treatment, 20 μl MTT solution was added to each well and incubated for 4 h in the incubator. Following which, the cell medium was removed and 200 μl DMSO was added to dissolve the purple formazan crystals in each well. Optical density values at 490 nm (OD490) were analyzed using a microplate spectrophotometer. The following equation was used to determine the percentage cell viability: Cell viability % = (OD490 of each group/average OD490 of the blank control group) × 100%.

RT-qPCR assay

The mRNA expression level was analyzed, as described in a previous study (Cui et al., 2016). Approximately 500 ng total RNA was reverse transcribed into cDNA using the Evo M-MLV RT Premix for the qPCR kit (Accurate Biotechnology, Hunan, China). RT-qPCR was performed using SYBR Green Premix Pro Taq HS qPCR kit (Accurate Biotechnology, Hunan, China). The primers were synthesized by Genewiz, Inc., Suzhou, China (Table 1).

Western blot analysis

Western blot analysis was conducted according to a previous study, with a slight modification (Cui et al., 2016). The cell lysates were collected, and the protein samples were separated using 10% SDS-PAGE, then transferred to PVDF membranes (Pall, USA). Subsequently, the membranes were blocked with blocking buffer (5% g/ml skimmed milk power (Anchor, New Zealand), which was dissolved in PBS containing

0.5% g/ml Tween-20 (PBST; Sangon Biotech Co., Ltd., Shanghai, China) for 1 h, then incubated with primary antibodies dissolved in 3% BSA overnight at 4°C. After the membrane was washed with PBST buffer (PBS added with 0.5% Tween-20) three times, the secondary antibodies (dissolved in blocking buffer) were added and incubated for 1 h. After washing again, the protein bands were visualized using enhanced chemiluminescence (Pierce™ ECL Western Blotting Substrate; Thermo Fisher Scientific, Inc., USA). The following primary antibodies were used: β-actin (mouse; 1:5000; A1978; Sigma-Aldrich), HIF-1α (mouse; 1:1000; 14179S; Cell Signaling Technology, Inc.), mTOR (rabbit; 1:1000; 2983; Cell Signal Technology, Inc.), and phosphorylated (p)-mTOR (rabbit; 1:1000; 5536; Cell Signal Technology Inc.).

ROS assay

The fluorescent probe, 2′, 7′-dichlorodihydrofluorescein diacetate (Beyotime Institute of Biotechnology) was used to detect reactive oxygen species (ROS) levels, the detected method as described in our previous study (Xu C. et al., 2018). The HL-1 cells (2×10^4 per well) were seeded into 24-well plates, then incubated with PA (0.25 mM) for 24 h to induce ROS generation. CAN (2.5 μg/ml) was simultaneously treated for 24 h to investigate the activity against ROS. The blank and untreated control cells were treated with an equal volume of DMSO or BSA solution. The fluorescent signal was measured using a fluorescence microscope (excitation wavelength of 485 nm; emission wavelength of 525 nm). Finally, quantitative analysis was conducted by ImageJ.

Immunofluorescence and confocal assay

The immunofluorescence assay in the HL-1 cells was performed as previously described (Xu C. et al., 2018). First, circular transparent glass slides (cat. no. 12-545-83; Fisherbrand™ microscope cover glass; Thermo Fisher Scientific, Inc. USA) were placed at the bottom of a 6-well plate. The cells, at a density of 2.5 × 105/well, were added to the surface of glass slides in a 6-well plate, then cultured in fresh medium. After 24 h of culture, the cells were divided into three groups: Normal untreated control group, PA (0.25 mM)-treated group, and PA (0.25 Mm)- and CAN (2.5 μg/ml)- treated group. After 24 h, the immobilized cells on the slides were washed with PBS, then fixed with 4% paraformaldehyde (Sangon Biotech, Shanghai, China) in PBS for 15 mins. The cells were washed with PBS three times, then incubated with 0.1% Triton X-100 in PBS for 15 min. After three washes with PBS, the cells were blocked with 3% BSA (Sangon Biotech, Shanghai, China) in PBS for 1 h. After blocking, the cells were incubated with p-mTOR (Ser2448) rabbit monoclonal antibody mAb (1:200; 5536S; Cell Signaling Technology, Inc., USA) and HIF-1α mouse monoclonal antibody (1:200; CST14179S; Cell Signaling Technology, Inc., USA) in 3% BSA for 1 h, then washed with PBS three times. Next, the cells were incubated with goat anti-rabbit IgG H&L (1:200; ab150077; Alexa Fluor® 488; Abcam, UK) or goat anti-mouse IgG H&L (1:100; ab150119; Alexa Fluor® 647; Abcam, UK) in 3% BSA for 1 h. The fluorescence in the cell was observed using confocal microscopy (Olympus, Corporation Japan) and analyzed using FV10-ASW Viewer v3.1 and ImageJ software.

Apoptosis assays

For the flow cytometry assays, the HL-1 cells (2×10^5/well) were cultured in 6-well plate. The cells were divided into three groups: Normal untreated control, PA (0.25 mM)- treated, and PA (0.25 Mm)- and CAN (2.5 μg/ml)-treated groups. After 24 h of treatment, the collected cells were fluorescently stained using the YF®488-Annexin V and PI Apoptosis commercial kit (Y6002; US Everbright Inc., Suzhou, Jiangsu, China). Flow cytometry was detected using a BD Accuri C6 flow cytometer (BD Biosciences, USA) and the results were analyzed using FlowJo v10.6.2 software.

For the confocal assay, the HL-1 cells (2×10^5/well) were seeded onto the surface of circular transparent glass slides in a 6-well plate and analyzed according to the confocal assay protocol, as described above. The cells on the slide were fluorescently stained using the YF®488-Annexin V and PI Apoptosis commercial kit (Y6002; US Everbright Inc, Suzhou, Jiangsu, China).

Pathway enrichment analysis

SwissTargetPrediction (http://www.swisstargetprediction.ch/) is a web server for small molecule drug target prediction (Daina et al., 2019). Using the web server, we obtained possible targets of CAN. ClueGo is a powerful tool for network analysis, annotation, and visualization. The predicted targets were analyzed using ClueGo 2.5.4 to enrich the pathway network for the Kyoto Encyclopedia of Genes and Genomes pathway database (Bindea et al., 2009) (the threshold was set at P < 0.05). GeneCards is a database

containing details of disease-related genes and proteins (16). The key words "diabetes" and "HF" were used in GeneCards to search for disease-related genes. From the results of the diabetes- and HF-related genes, we selected the top 200 genes and analyzed them using ClueGo (the threshold was set at $P < 0.001$). The enrichment results and intersection analysis were conducted using Origin Pro 2018c.

Molecular docking assay

SwissDock is an online sever for small molecule-protein docking (Grosdidier et al., 2011). The mTOR crystal structure was obtained using the Protein Data Bank (PDB ID: 4DRI). The molecular docking model and affinity energy of CAN,DAP,EMP and RAPA with mTOR were analyzed using SwissDock (www.swissdock.ch) and the results were visualized using the software, Chimera v1.14 (Pettersen et al., 2004).

Affinity chromatography

Affinity chromatography was conducted according to a previous study (Chen et al., 2020) with a slight modification.

Preparation of the drug: CAN, DAP and EMP 5 mg was dissolved in 0.35 ml of 80% ethanol, while sucrose (3 mg) was dissolved in 0.35 ml of 40% ethanol. The two solutions were dropped into 0.25 ml of 8 mg/ml sodium periodate (Sangon Biotech Co., Ltd.) solution and left for 1 h for the reaction to occur. Following which, 0.5 ml of 100 mM sodium carbonate buffer (pH, 9) was added to the two solutions.

Preparation of the affinity chromatography column: Two 5 ml centrifuge chromatography tubes (Thermo Fisher Scientific, Inc., USA) were prepared, and 1 ml resin (Carboxylink™ Coupling Gel; Thermo Fisher Scientific, Inc., USA) was transferred into one of the tubes. The supernatants were removed using centrifugation at 1000 rpm for 20 s and washed with deionized water three times.

Linking the drug onto the column: 0.375 ml of 4 mg/ml sodium borohydride solution (Sangon Biotech Co., Ltd.) was added into the aforementioned two resin tubes, mixed in a shaker, and left to react for 4 h. The cover of the tube was opened every half an hour to release the gas generated in the reaction.

Affinity chromatography: The HL-1 cells were cultured in a 10-cm plate. The cell lysates were collected and loaded into the prepared chromatography resin tubes and incubated overnight at 4°C. The proteins bound to the resin was separated using SDS-PAGE and identified using Coomassie brilliant blue staining and western blot analysis.

QUANTIFICATION AND STATISTICAL ANALYSIS

All the data are repeated three or more times independently and presented as the mean ± SD. Unpaired t-test (two tailed) was used when comparing two groups and GraphPad Prism v8 software. One-way ANOVA with Tukey's post hoc test was used for multiple comparisons and SPSS v22 software. $P < 0.05$ was considered to indicate a statistically significant difference.